

Quantitative Determination of Adsorbate-Adsorbate Interactions

L. Österlund, M. Ø. Pedersen, I. Stensgaard, E. Lægsgaard, and F. Besenbacher*

CAMP and Institute of Physics and Astronomy, University of Aarhus, DK-8000 Aarhus C, Denmark

(Received 18 June 1999)

A new concept called configuration distribution analysis is introduced to extract quantitative information on adsorbate-adsorbate interactions from high-resolution scanning tunneling microscopy data. From atom-resolved nitrogen island configurations on an Fe(100) surface we show that the propensity to form small, compact $c(2 \times 2)$ nitrogen islands is due to a nearest neighbor repulsion and next-nearest neighbor attraction. We demonstrate the importance of including many-body terms and elastic interactions to account for the detailed description of the island distribution.

PACS numbers: 68.35.Dv, 34.20.Cf, 82.60.Nh

Interatomic interactions are of utmost importance for the description of condensed matter. However, it is a nontrivial problem to obtain quantitative information on the interatomic interactions, which in general are of many-body nature. The surface might be the ideal playground to study interatomic interactions, since the symmetry of the problem is reduced to two dimensions, and it is possible to monitor individual atoms directly [1–5]. The structures that form when atoms and molecules adsorb on solid surfaces are often ordered, and a comprehensive database is now emerging [6]. The very existence of long-range ordered structures, with repeat distances longer than an atomic diameter, implies that adsorbate-adsorbate interactions are important and can make distant sites become energetically favorable.

Traditionally, a pair distribution analysis has been used to analyze the observed adsorbate distribution, from which a pair potential is obtained by means of, e.g., a pair correlation function or a lattice gas analysis [2–4,7–9]. The inherent drawback of this method is that it only represents a mean field approach when more than two atoms are considered, and that it is not possible *a priori* to distinguish local inhomogeneities in the particle distribution that may favor a particular arrangement of atoms within islands. Many-body terms, which are known to be important in the theoretical descriptions of, e.g., phase diagrams of surface structures, are thus most often ignored [10]. Furthermore, it is generally difficult to directly relate the pair correlation function to a real value of the pair potential, since for ensembles of atoms, the latter contains non-negligible contributions of the entropy of the system.

In the present Letter, we introduce a new concept of island *configuration distribution analysis* (CDA) to extract reliable values for adsorbate-adsorbate interactions from a detailed analysis of high-resolution scanning tunneling microscopy (STM) data. For the first time, quantitative values of adsorbate-adsorbate interactions that reproduce the equilibrium atomic arrangements of adsorbate islands on a metal surface are obtained, exemplified by the case nitrogen on Fe(100). Besides providing quantitative information of a nearest neighbor repulsion and next-

nearest neighbor attraction, this method allows direct access of many-body effects and elastic interactions.

Using a homebuilt STM [5], high-resolution STM images were obtained for N coverages up to 0.15 monolayers ($\Theta = 0.15$). To avoid the intrinsic difficulties in cleaning Fe surfaces, we used a Fe(100) thin film grown by deposition of Fe on a MgO(0001) substrate. The N adatoms were adsorbed by thermal decomposition of NH_3 at 670 K to circumvent the very low dissociative sticking probability of N_2 and maintain clean deposition conditions. After exposure, the surface was cooled to room temperature and transferred to the STM for imaging.

Figure 1 shows an STM image at $\Theta = 0.108$. Only small embryos of $c(2 \times 2)$ islands are observed, which is representative for the adatom distribution at $T = 298$ K [11]. The N atoms are imaged as depressions in

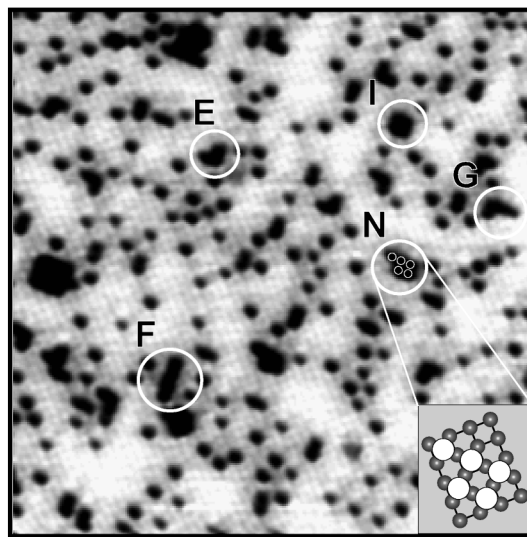


FIG. 1. An STM image ($160 \times 154 \text{ \AA}^2$) displaying small islands of N atoms with atomic resolution of both the individual islands and the Fe(100) lattice at $\Theta = 0.108$. The image is recorded in constant current mode ($I = 1.2 \text{ nA}$, $V = 0.175 \text{ V}$) at $T = 298 \text{ K}$. A few islands are labeled according to the schematic drawing in Fig. 3B. The inset shows a ball model of a pentamer (type N), which is also indicated in the STM image with white circles.

agreement with calculations [12]. The fact that we can simultaneously resolve both the N adatoms *and* the Fe lattice implies that (i) we can unequivocally confirm that the N atoms are adsorbed in the fourfold hollow sites [11,13], and (ii) we can directly convert the STM images into a discrete site map without having to impose a lattice grid according to the observed adatom positions.

In the following we introduce a two-dimensional site map around each adatom with possible N adsorption sites located at r_j in units of the Fe lattice constant ($a = 2.87 \text{ \AA}$). Thus, $j = 1$ denotes nearest neighbor sites ($r_1 = 1$), $j = 2$ next-nearest neighbor sites ($r_2 = \sqrt{2}$), etc. (Fig. 2). The conventional pair correlation analysis provides a measure of the average number of pairs of N adatoms as a function of interparticle separation. From the STM data, the discrete pair correlation function, $g(j)$, has been determined at a range of different coverages between $\Theta = 0.037$ and $\Theta = 0.15$. Analysis of the data ensures us that at all coverages the particle distribution is homogeneous, i.e., the function $g(j)$ is isotropic, and that the system is at *equilibrium* [14], which justifies a conventional pair correlation analysis [8,9]. We will focus on the low coverage data where the entropic contributions are small, and hence provide the most direct information on the pair potential. Figure 2 shows $g(j)$ vs neighbor site, j , for $\Theta = 0.037$. There are very few nearest neighbor sites ($j = 1$) occupied, and there is an enhanced probability of finding N atoms at site $j = 2$. At sites $j > 4$ there are no significant deviations from a random distribution ($g = 1$). In the limit of zero coverage, i.e., when the entropic contribution vanishes, $g(j)$ and the pair potential, $V_j^{(2)}$, are

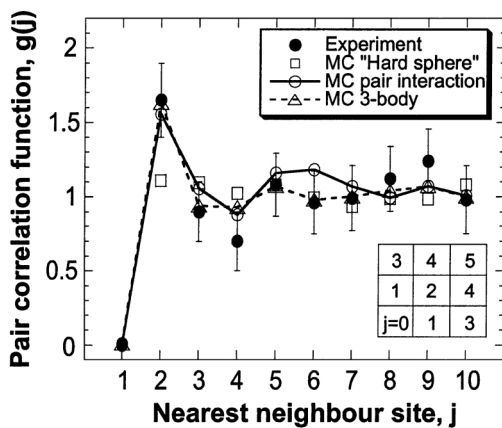







FIG. 2. Experimental and simulated pair correlation function, $g(j)$, vs neighbor site, labeled by j , at $\Theta = 0.037$. The normalization ensures that $g \rightarrow 1$ as $j \rightarrow \infty$. The experimental error bars indicate the statistical spread from 17 independent measurements, which include a total of 1066 atoms. The MC simulations were performed on a 150×150 lattice grid assuming (i) hard-sphere repulsion ($V_1^{(2)} = \infty$, and $V_{j>1}^{(2)} = 0$), (ii) additive pair interactions, and (iii) three-body interactions. The best fit potentials obtained in the latter cases are listed in Table I.

related by $V_j^{(2)} = -kT \ln(g(j))$. A simple estimate then yields $V_1^{(2)} = 0.130 \text{ eV}$ and $V_2^{(2)} = -0.013 \text{ eV}$, respectively. Since the accuracy of these estimates depends on the low coverage data, which in turn are difficult to access experimentally with good statistics, we have in addition performed Monte Carlo (MC) simulations using both a hard sphere potential, and a three-parameter least squares fit procedure. In the latter simulations, we have determined the parameters $V_1^{(2)}$, $V_2^{(2)}$, and $V_3^{(2)}$ that simultaneously fit *all* data between $\Theta = 0.037$ and $\Theta = 0.15$. We note that the enhancement at site $j = 2$ cannot be explained simply by entropic forces as simulated by the hard sphere model, but an additional attractive interaction at site $j = 2$ must be included to fit the experimental data with reasonable accuracy. The best fit MC parameters (Table I) are in good agreement with those from the simple estimate above.

Despite the apparently good agreement between the experiments and the simulations, it is important to stress that the pair correlation analysis fails to account for the observed island shapes and the island size distribution as will be discussed below. In the following we will therefore go beyond the pair correlation analysis and introduce the new CDA method to extract adsorbate-adsorbate interactions [15]. This analysis thus takes into account the conditional probabilities in the site occupation distribution; i.e., many-body effects are accounted for on a microscopic level. Depicted in Fig. 3A is the likelihood of finding a particular island configuration normalized to the corresponding

TABLE I. Compilation of the adsorbate-adsorbate interaction potentials obtained by the pair correlation analysis ($\Theta = 0.037$) and CDA ($\Theta = 0.108$), respectively. The CDA potentials are obtained by MC simulations using Eq. (1), and further refined by a least-squares fit to the island size distribution in Fig. 4. The best fit elastic constants are $C/a^3 = 0.08 \text{ eV}$ and $C/a^3 = 0.15 \text{ eV}$ for the pair and three-body interaction potentials, respectively. The best fit is obtained by the three-body CDA result. The CDA provides a very narrow acceptable parameter space for the best fit potentials. To obtain ϵ values within 10% of the best fit three-body result requires that each potential cannot vary more than ca. 6 meV. The inclusion of site $j = 3$ gives no significant difference in the three-body CDA (value in parentheses).

	Pair correlation analysis		Monte Carlo CDA	
	$-kT \ln(g(j))$ [eV]	Monte Carlo [eV]	Pair interactions [eV]	Three-body interactions [eV]
$V_1^{(2)}$ 	0.13	0.14	0.13	0.13
$V_2^{(2)}$ 	-0.013	-0.023	-0.038	-0.018
$V_3^{(2)}$ 		0.003	0.010	0.019 (0.015)
$V_1^{(3)}$ 				-0.012
$V_2^{(3)}$ 				0.006

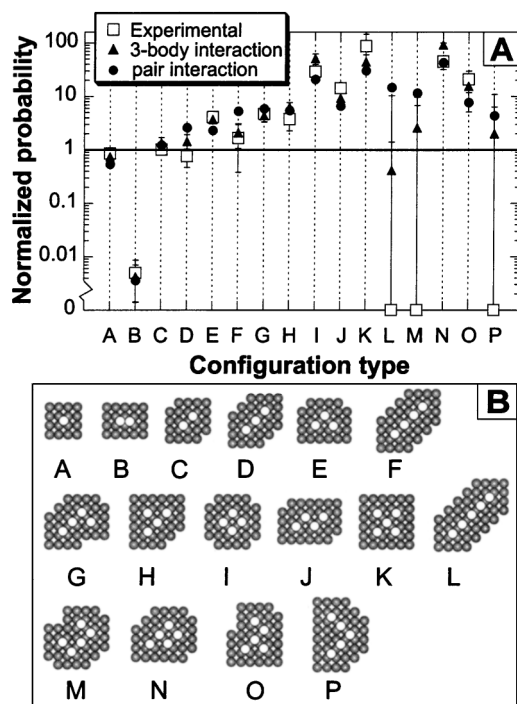


FIG. 3. (A) The likelihood of finding a particular island configuration, labeled by the letters *A* to *P*, at $\Theta = 0.108$. Note the logarithmic scale. The probabilities are normalized to the probability of finding a corresponding configuration for an ensemble of randomly distributed particles. The hollow squares represent the experimental data, while the filled symbols show the results from MC simulations. The solid triangles (circles) are the best fit obtained using three-body (pair) interactions. The best fit parameters are listed in Table I. The error bars indicate the statistical spread of each configuration, or in those cases where the configuration was not found (e.g., type *L*), the error bars represent the resolution of the finite experimental data set. The simulated CDA represents the average over 10 MC runs, and the standard deviation of the best fit result is explicitly shown. For clarity, only a selection of the full configuration distribution is shown. The full CDA includes 1513 islands containing up to 10 atoms. (B) Schematic illustration of the island configuration types used in panel A. Each depicted “cluster” *A* to *P* also defines the filled and empty sites defining each island.

probability for an ensemble of randomly distributed particles. Figure 4 shows the island size distribution, which complements the data in Fig. 3A in the sense that it emphasizes the relative population of different island sizes. The most distinctive features of the experimental data are the following: (i) An enhanced probability of finding compact $c(2 \times 2)$ islands, e.g., structures of type *E*, *I*, *K*, *N*, and *O*; at $\Theta = 0.108$ the only islands consisting of more than five atoms which we observe are compact $c(2 \times 2)$ islands (cf. Fig. 1). The difference between, e.g., structures *D* and *E* indicates that simple bond counting arguments based on pairwise interactions up to $j = 2$ cannot explain the experimental data. (ii) A relatively smaller probability of finding open islands consisting of single-stranded chains of atoms (e.g., type *D*, *L*, *M*, and *P*).

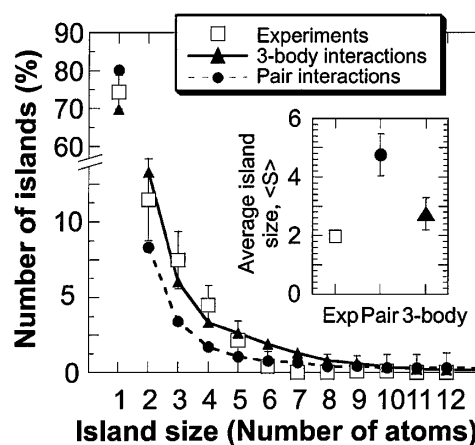


FIG. 4. Comparison of the experimental and simulated island size distribution at $\Theta = 0.108$. The inset shows the average island sizes defined by $\langle S \rangle = \sum_s s N_s / \sum_s N_s$, where N_s is the island density (per adsorption site) of size s . For the three-body interaction potentials, the average island size is $\langle S \rangle = 2.7 \pm 0.4$, which is close to the experimental value $\langle S \rangle = 2.0$, whereas for the pair interaction potentials, the average island size is too large ($\langle S \rangle = 4.8 \pm 0.7$).

(iii) Only small islands are observed (the average island size, $\langle S \rangle = 2.0$ at $\Theta = 0.108$). To quantitatively determine the form of the interaction potential that best describes the observed island configuration distribution, we have performed MC simulations using a many-body lattice gas Hamiltonian, viz.

$$H = H_0 + \sum_k \sum_{l>k} V_{kl}^{(2)} n_k n_l + \sum_k \sum_{l>k} \sum_{m>l} V_{klm}^{(3)} n_k n_l n_m + \dots + \text{elastic terms.} \quad (1)$$

Here the summation runs over all sites labeled by a single index k , H_0 is the Hamiltonian of the system without adsorbate interactions, n_k is the occupation number (1 or 0 depending on whether the site is filled or not), and $V_{kl}^{(2)}$ and $V_{klm}^{(3)}$ are the pair and three-body interaction potentials, respectively (see Table I for our shorthand notation of the relevant potentials). Elastic interactions are explicitly included at sites $j \geq 3$ by adding an extra term C/r_j^3 (which is appropriate in the asymptotic limit), where C is a constant describing the elastic properties of the system [16]. It is, however, difficult to disentangle the electronic and elastic contribution at short distances, especially when there are significant relaxation effects of the neighboring lattice atoms [1]. As a test we have therefore also extended the region around each adatom where the elastic term is not included explicitly. No significant difference is, however, obtained in these simulations. The result in Fig. 3A is obtained for interactions extending to next-nearest neighbors ($j = 2$). In Table I is also shown the result if $j = 3$ is included in the analysis. It is seen that a three-body (trio)

interaction potential gives a significantly better fit than if only pair interactions are included. A rigorous error analysis further clarifies this point. The relative error of the simulated CDA distributions compared to the experimental CDA distribution is $\epsilon = 0.39$ and $\epsilon = 0.99$, respectively, for the full three-body and pair interaction fit, where ϵ is defined as $\epsilon = N^{-1} \sum_N |R_i - R_{\text{exp}}| / \min(R_i, R_{\text{exp}})$, where N is the number of configurations, and R_i and R_{exp} are the simulated and experimental probabilities in Fig. 3A, respectively. Taking the spread in the experimental and simulated results into account we find that 81% of the three-body data points are within the statistical spread, while the corresponding value for the pair interaction is only 50%. The best fit three-body potentials $V_1^{(3)}$ and $V_2^{(3)}$ favor compact $c(2 \times 2)$ islands against open islands. These potentials are small but important, since they are of the order $\frac{1}{2}kT$. The interaction potentials obtained with the CDA give an excellent fit to the pair distribution in Fig. 2, which explicitly shows that the information contained in Fig. 3 includes the information in Fig. 2, but not vice versa.

To complete the CDA, the island size distribution must be included. This adds an extra dimension to the analysis, which accounts for the relative abundance of the different configurations in Fig. 3. Figure 4 clearly shows that the three-body result gives an excellent agreement with experiments, while pair interactions yield too few small islands and too many large islands as discussed above. The island size distribution is very sensitive to the elastic interactions and allows us to further refine the overall best fit parameters (Table I). This behavior is consistent with *ab initio* density functional theory calculations [13], which have shown that the elastic strain induced by N adsorption on iron is substantial. We may compare our best fit value of the elastic constant $C/a^3 = 0.15$ eV with what the continuum theory predicts. According to Lau and Kohn [16], the latter is given by $E_{\text{int}}^{\text{elastic}} = \pi(1 - \sigma^2)a^2 f^2 / Er^3$, where $\sigma = 0.29$ is the Poisson ratio, $E = 211$ GPa is the Young's modulus, and $f = 7.4 \times 10^{-10}$ N is the force caused by the atom on the substrate [13]. This estimate yields $C/a^3 = 0.16$ eV, which is remarkably close to what we obtained from the CDA above. An estimate of the electronic contribution to the total interaction potential may be obtained at site $j = 3$, where the elastic interactions are explicitly included. Using the best fit value of $C/a^3 = 0.15$ eV, we obtain $E_{\text{int}}^{\text{elastic}} = 19$ meV and by comparison with Table I (value in parentheses), we see that the electronic interaction at site $j = 3$ is only about -4 meV. At site $j = 2$, the elastic term is expected to be much larger, but the net result is still a pair attraction of -18 meV, which means that the electronic interaction must be large at this site. Thus, we conclude that the electronic interaction

is short ranged and that it has a significant influence that reaches mainly to next-nearest neighbor sites. It is interesting to note that the radius of the N-induced depressions seen in the STM images is ~ 4.1 Å. This is in perfect agreement with an electronic perturbation of the substrate, i.e., an indirect interaction, that extends to next-nearest neighbor sites.

In summary, this work demonstrates how STM can be used to assess the general form of interparticle interactions on surfaces with a new method called the CDA. This work should have the potential of stimulating similar efforts in understanding the formation of overlayer structures, and should provide a hallmark for *ab initio* theoretical calculations.

We acknowledge valuable discussions with J.K. Nørskov and M. Mavrikakis, as well as the financial support from the Danish National Research Foundation through the Center of Atomic-Scale Materials Physics (CAMP). We thank Jaques Chevalier for preparation of the Fe thin films.

*Corresponding author.

Electronic address: fbe@ifa.au.dk

- [1] T.L. Einstein and J.R. Schrieffer, Phys. Rev. B **7**, 3629 (1973); T.L. Einstein, in *Handbook of Surface Science I*, edited by W.N. Unertl (Elsevier, Amsterdam, 1996), Vol. 1, p. 577.
- [2] G. Ehrlich, Surf. Sci. **299/300**, 6281 (1994).
- [3] R. Gomer, Rep. Prog. Phys. **53**, 917 (1990).
- [4] T.T. Tsong, Rep. Prog. Phys. **51**, 759 (1988).
- [5] F. Besenbacher, Rep. Prog. Phys. **59**, 1737 (1996).
- [6] G.A. Somorjai, *Introduction to Surface Chemistry and Catalysis* (John Wiley & Sons, New York, 1994).
- [7] T.-M. Lu *et al.*, Phys. Rev. Lett. **39**, 411 (1977).
- [8] J.C. Dunphy *et al.*, J. Vac. Sci. Technol. A **11**, 2145 (1993).
- [9] J. Trost *et al.*, Phys. Rev. B **54**, 17 850 (1996).
- [10] K. Binder and D.P. Landau, Surf. Sci. **108**, 503 (1981); B.N.J. Persson, Surf. Sci. Rep. **15**, 1 (1992).
- [11] R. Imbihl *et al.*, Surf. Sci. **123**, 129 (1982).
- [12] P. Sautet, Surf. Sci. **374**, 506 (1997).
- [13] J.J. Mortensen *et al.*, Surf. Sci. **422**, 8 (1999).
- [14] The measured diffusion coefficient is 3×10^{-10} cm²/s at 670 K [M.Ø. Pedersen *et al.* (to be published)], which is sufficient for the N atoms to reach equilibrium during the deposition time. We have in addition performed MC simulations (see below) to ensure that no nonequilibrium structures are "frozen" in when the surface is cooled down. At all temperatures the system is above the melting point as judged by the smooth variation of the energy fluctuations $(\langle E^2 \rangle - \langle E \rangle^2)$ vs temperature.
- [15] A comprehensive treatment of the CDA method will be presented elsewhere.
- [16] K.H. Lau and W. Kohn, Surf. Sci. **65**, 607 (1977).